



Aligning carbon nanotubes using bulk acoustic waves to reinforce polymer composites



Michael D. Haslam, Bart Raeymaekers*

Department of Mechanical Engineering, University of Utah, Salt Lake City, UT 84112, USA

ARTICLE INFO

Article history:

Received 3 November 2012

Received in revised form 28 November 2013

Accepted 22 December 2013

Available online 31 December 2013

Keywords:

A. Discontinuous reinforcement

A. Polymer–matrix composites (PMCs)

A. Nano-structures

ABSTRACT

Bulk acoustic waves (BAWs) are used to align multi-walled carbon nanotubes (MWCNTs) in polymer composite materials. MWCNTs are first dispersed in the liquid state of a thermoset resin and aligned using standing BAWs. Cross-linking of the resin fixates the aligned MWCNTs in the polymer matrix material. We have quantified the alignment obtained with this method on the macro, micro, and nanoscale, and it is found to be similar to other alignment techniques such as stretching, slicing, and wet spinning. The elastic modulus and ultimate tensile strength of composite material specimens with aligned MWCNTs, fabricated using this technique, are evaluated and compared with specimens consisting of randomly oriented MWCNTs and resin material without MWCNTs. Different MWCNT loading rates are considered. The elastic modulus of composite material specimens with only 0.15 weight percent aligned MWCNTs is observed to be 44% higher than specimens with randomly oriented MWCNTs, and 51% higher than specimens without MWCNTs. However, further increasing the MWCNT loading rate does not significantly increase the elastic modulus and ultimate tensile strength, likely because of insufficient dispersion of MWCNTs in the thermoset matrix material.

© 2013 Elsevier Ltd. All rights reserved.

1. Introduction

Carbon nanotubes (CNTs) exhibit extraordinary mechanical properties [1,2]. Attempting to implement CNTs as nanoscale reinforcement in composite materials or fibers is an active research area [3–12]. Several parameters are critical when manufacturing composite materials with CNT reinforcement, such as dispersion of the CNTs in the polymer matrix [13,14], bonding between the CNTs and the matrix material [15–18], and alignment of the CNTs in the direction of the applied external loading [19,20]. In this paper, we focus on the alignment of the CNTs in the polymer matrix.

A variety of techniques to align CNTs have been documented in the literature, including methods based on stretching [21], magnetic [22–25] or electrostatic forces [26], slicing [27], liquid crystals [28], shear flow [29], and surface acoustic waves [30]. Fibers reinforced with aligned CNTs have been produced using wet spinning [31], melt spinning [32–34], and direct spinning [35]. These fibers must be further processed into a bulk composite material. While these are effective methods to align CNTs, scalability for use as a manufacturing technique of macroscale specimens is often the limiting factor.

This paper attempts to address this limitation and presents a novel technique, based on bulk acoustic waves (BAWs), to align

CNTs in a polymer matrix. BAWs have previously been used to manipulate microscale particles [36–39], cells [40,41], and nanoparticles [42]. Here, multi-walled carbon nanotubes (MWCNTs) are dispersed in the liquid state of a thermoset resin and subsequently aligned and organized into parallel lines by means of BAWs. The obtained pattern of MWCNTs is fixated by cross-linking the resin, which yields a polymer composite material reinforced with aligned MWCNTs. The alignment is experimentally quantified on the macro, micro, and nanoscale. The elastic modulus and ultimate tensile strength of the composite material specimens with aligned MWCNTs are measured in the direction of the MWCNT alignment, and compared against composite material specimens consisting of randomly oriented MWCNTs and pure resin material without MWCNTs. Different MWCNT loading rates are considered.

2. Experimental methods

2.1. Apparatus

Fig. 1 shows a schematic of the experimental apparatus. A dog-bone shaped reservoir is machined from high density polyethylene, which displays low adhesion to the polymer matrix material [43]. The reservoir is mounted on a glass base. Two parallel lead zirconate titanate (PZT-5) plates are embedded in recess slots in the side walls of the reservoir, and oppose each other over the entire 18 mm gauge length. The dog-bone specimen is 68 mm long,

* Corresponding author. Tel.: +1 801 585 7594; fax: +1 801 585 9826.

E-mail address: bart.raeymaekers@utah.edu (B. Raeymaekers).

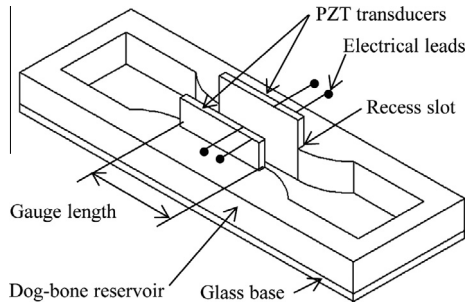


Fig. 1. Schematic of the experimental apparatus to manufacture dog-bone composite material specimens, with aligned MWCNTs in the gauge length.

5 mm thick, and 7.5 mm wide in the gauge section (measured between the PZT plates). These dimensions are chosen to resemble an ASTM D638 Type V plastic specimen. The PZT material (18 × 12 mm) has a center frequency of 1.5 MHz. The PZT transducers create BAWs in the reservoir to align the MWCNTs in the gauge section of the dog-bone specimen.

2.2. Aligning CNTs using bulk acoustic waves

The pressure P of a one-dimensional BAW is represented as [44]:

$$P(x, t) = P_a \cos(\omega t - kx) + P_a \cos(\omega t + kx) \quad (1)$$

where P_a is the pressure amplitude, $k = 2\pi/\lambda$ is the wave number, λ is the wave length, ω is the angular frequency, t is the time, and x is the distance from the transducer. The acoustic radiation force F associated with the pressure wave, acting on a cylinder, has been shown to be of the following form [44–47].

$$\frac{F}{L} = \left\{ \frac{(1 - \beta)/(1 + \beta)}{2} + 1 \right\} \nu \omega \left(\frac{P_a^2}{\rho_0 c^3} \right) \sin(2kx) \quad (2)$$

where L is the length of the cylinder. The amplitude of the radiation force is a function of the pressure wave amplitude P_a , the volume of the cylinder per unit length ν , the density of the medium ρ_0 , the density of the cylinder ρ_1 , $\beta = \rho_0/\rho_1$, the sound speed c of the medium, and the angular frequency ω . Fig. 2 illustrates the normalized magnitude of a pressure wave (dashed line) and the corresponding acoustic radiation force (solid line) as a function of the distance from the PZT transducer, nondimensionalized with the wave length λ of the BAW. The location of the nodes and antinodes is indicated, and the horizontal bold arrows denote the direction in which the

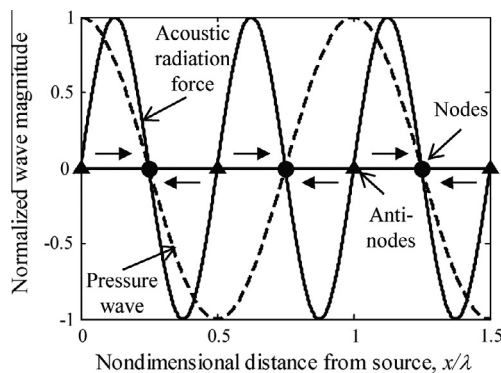


Fig. 2. Node and antinode locations of a pressure wave and the corresponding acoustic radiation force (see Eqs. (1) and (2)) with arrows showing the direction in which MWCNTs are driven.

MWCNTs are driven; a positive radiation force induces a displacement along the positive x -axis and vice versa [42].

Fig. 3 shows the manufacturing process to create polymer composite material specimens with aligned MWCNTs. Virgin MWCNTs with a diameter of 50–80 nm and length of 10–20 μm are added to part A of a two-part, low-viscosity, fast curing thermoset resin (Smooth-Cast 300 thermoset, Smooth-On Inc.) (Fig. 3(a)), and dispersed by means of bath sonication (Fig. 3(b)). Part B of the resin is then added (Fig. 3(c)) prior to transferring the mixture to the dog-bone shaped reservoir (Fig. 3(d)). The sound speed of the thermoset resin c is 1353 m/s at room temperature (20 °C) and is determined with a pulse echo time-of-flight measurement [48]. The viscosity of the liquid resin at room temperature is 0.008 Pa s, and it is noted that the viscosity of the polymer increases with increasing MWCNT loading. A standing BAW is created between the two opposing PZT transducers at a frequency close to their resonance frequency, to maximize the amplitude of the pressure wave and, correspondingly, the magnitude of the acoustic radiation force (see Eq. (2)). This force aligns the MWCNTs and drives them to the nodes of the standing BAW (Fig. 3(e)), when it exceeds the drag force acting on the MWCNTs [38]. The PZT transducers are energized by a function generator (Tektronix, AFG 3102), amplified by a 45 dB 50 W RF power amplifier (electronic navigation industries, 440LA). By controlling the location of the nodes of the standing BAW, which depends on the wave length or frequency of the wave and the sound speed in the polymer matrix material, one can control the locations where the MWCNTs assemble and align. Cross-linking of the mixture starts immediately following the addition of part B of the resin. The sample is extracted from the reservoir upon completion of the cross-linking process (Fig. 3(f)).

Fig. 4(a) depicts a typical dog-bone specimen with one weight percent (wt%) aligned MWCNTs, fabricated using BAWs with a frequency of 1.477 MHz. Fig. 4(b) shows a detail of the gauge section with parallel lines of aligned and clustered MWCNTs. The surface of the specimen is locally polished to reveal the alignment of the MWCNTs. Details of the nanoscale alignment of the MWCNTs are shown in Section 3. The spacing between two lines of aligned MWCNTs is 458 μm , which is expected based on the sound speed of the resin matrix material (in liquid state), and the occurrence of two nodes per wave length as shown in Fig. 2. Dog-bone specimens with randomly oriented MWCNTs are fabricated using the same process as outlined in Fig. 3, with the exception of the step in which the MWCNTs are aligned.

3. Results and discussion

3.1. Quantifying MWCNT alignment

The orientation factor H [49] quantifies the alignment of the MWCNTs, and is based on the average angle ϕ between the axis of the MWCNTs and the composite axis. The composite axis is defined as the axis in which alignment is desired, and in which the external load will be applied. Perfect alignment results in $H = 1$ ($\phi = 0^\circ$). If all fiber axes are oriented orthogonal to the composite axis ($\phi = 90^\circ$), $H = -0.5$, and for randomly oriented fibers ($\phi = 45^\circ$), $H = 0.25$. This method has previously been used to quantify fiber alignment in nanostructured polymer composite materials e.g. [50–52], and H is computed as:

$$H = \frac{1}{2} (3 \cos^2 \phi - 1) \quad (3)$$

To quantify the macroscale alignment of clusters of MWCNTs in the composite material specimen, a 6.7 by 5.0 mm section of the specimen is photographed through a trinocular stereo zoom microscope (AmScope MT500). The grayscale digital image is binarized

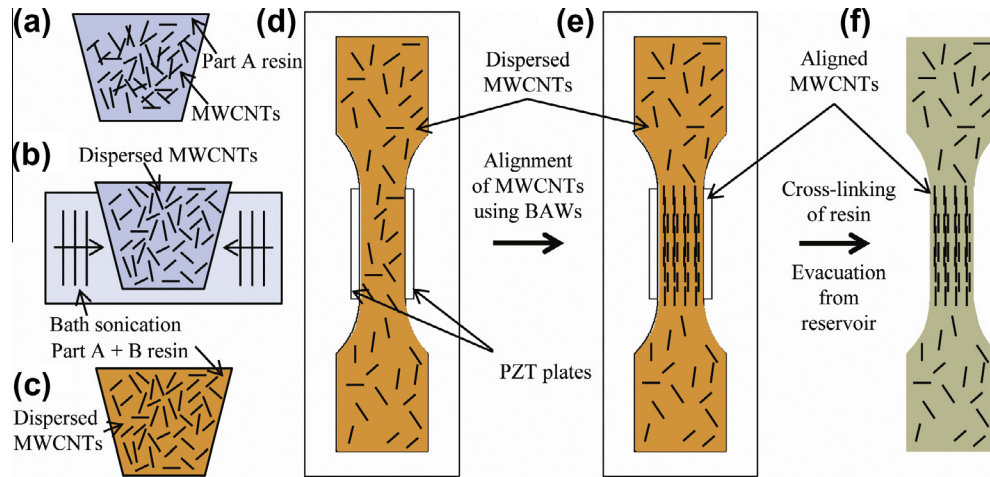


Fig. 3. Manufacturing process of a dog-bone shaped composite material specimen with aligned MWCNTs.

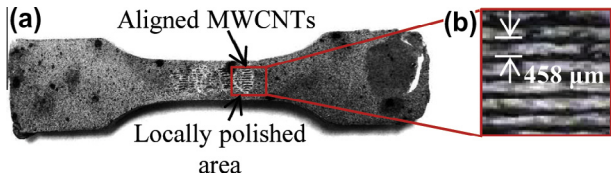


Fig. 4. (a) Dog-bone sample with 1 wt% aligned MWCNTs and (b) locally polished surface reveals detail of the parallel lines of aligned MWCNTs obtained using BAWs at a frequency of 1.477 MHz.

with a luminance cut off of 0.20, depicting resin in white and MWCNTs in black. This image is then overlaid with gray lines through each MWCNT cluster axis. Fig. 5 displays a typical example of the unprocessed (Fig. 5(a)) and binary image (Fig. 5(b)) for the 1 wt% loading rate specimen shown in Fig. 4. Table 1 shows H for three specimens with different loading rates, demonstrating excellent macroscale alignment of the clusters of MWCNTs in the thermoset resin.

Quantifying the alignment in the polymer matrix requires slicing the hardened polymer, which is known to provide alignment [27], and could corrupt the measurement. Hence, micro- and nanoscale alignment using BAWs is demonstrated by aligning MWCNTs in a 0.01 wt% aqueous solution of MWCNTs, rather than in a polymer matrix. The water is allowed to evaporate, depositing the aligned MWCNTs on the glass base of the reservoir by means of gravity. The alignment is evaluated using a scanning electron microscope (SEM). The small loading rate is chosen to improve

Table 1
Orientation factor H for specimens with different MWCNT loading rate.

Specimen (wt%)	ϕ (°)	H
0.50	2.51	0.997
1.00	3.45	0.995
2.00	5.02	0.989

dispersion of the MWCNTs in the solution and reduce entanglement. Fig. 6(a) shows the aligned MWCNTs at a 500 nm magnification scale, while Fig. 6(b) depicts a single line of MWCNTs, representing a nodal line of the original standing pressure wave, at a 50 μm magnification scale. These images are overlaid with gray lines to determine the orientation factor.

While Fig. 6(a) certainly displays several MWCNTs that are not in good alignment, an orientation factor of $H = 0.776$ is obtained, which is comparable to values reported in the literature for other CNT alignment methods such as mechanical stretching (H of approximately 0.70 [21]) and wet spinning ($H = 0.85$ [51]). However, compared to these alternative methods the BAW alignment technique accommodates scaling to fabrication of large composite specimens. Even on the nanoscale, good alignment is obtained with the BAW alignment technique. We speculate that the nanoscale alignment would improve further if shorter and thinner single-walled carbon nanotubes (SWCNTs) are used (as opposed to MWCNTs). Shorter SWCNTs are less likely to entangle, thus facilitating dispersion, manipulation, and alignment. Fig. 6(b) shows overall alignment similar to the macroscale images with $H = 0.973$.

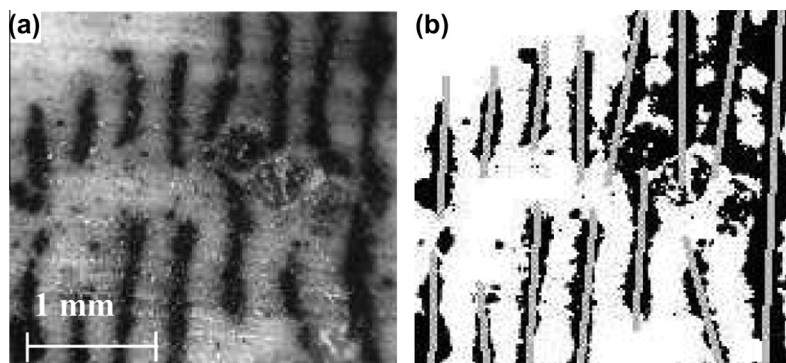


Fig. 5. (a) Unprocessed image and (b) processed image showing black MWCNT clusters overlaid with gray lines along their axis for determining the orientation factor H of the MWCNTs in the specimen.

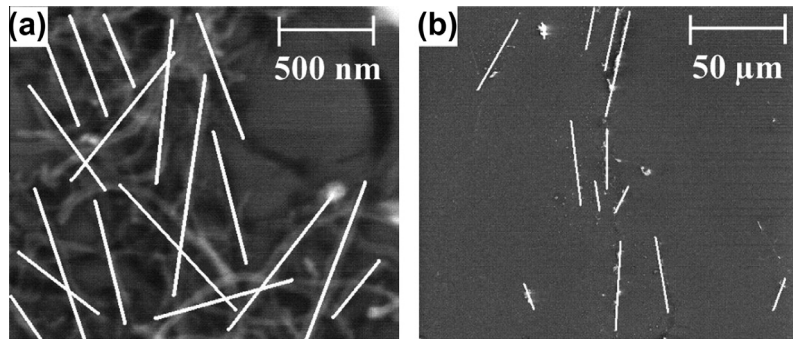


Fig. 6. Processed SEM images at (a) 500 nm ($H = 0.776$) and (b) 50 μm ($H = 0.973$) magnification scale, with gray lines overlaying the longitudinal axis of the MWCNTs.

The viscosity of the medium (resin) is a critical parameter for the BAW alignment technique, because it affects the drag force acting on the MWCNTs. Alignment of the MWCNTs only occurs if the acoustic radiation force exceeds the drag force. A chart that maps the operating domain for manipulation of spherical nanoparticles with BAWs was previously presented in [42]. Despite the ultra-low viscosity (0.008 Pa s) of the thermoset resin, the MWCNTs are observed to stay in solution, and do not gravitate towards the base of the reservoir during the time-span of the MWCNT alignment. As the cross-linking process starts, the viscosity of the mixture increases, and aligning and displacing MWCNTs becomes increasingly difficult. During our experiments, the standing BAW is maintained for 30–90 s to align the MWCNTs.

3.2. Static testing

Traditional tensile testing of the dog-bone specimens is performed in a load frame (Instron 5985) to determine the change in mechanical properties afforded by the alignment of MWCNTs in a polymer matrix. A displacement rate of 2 mm/min is used and strain is measured with an extensometer (MTS 632.26 C-20) while the load is simultaneously monitored using a 1 kN load cell. The elastic modulus E_c and the ultimate tensile strength $\sigma_{\text{UTS},c}$ of the composite material specimen is derived from the stress–strain curve for each specimen.

E_c and $\sigma_{\text{UTS},c}$ of the composite material specimens with aligned MWCNTs are compared with composite material specimens with randomly oriented MWCNTs and specimens without MWCNTs. MWCNT loading rates of 0.15, 0.5, and 1 weight percent (wt%) are used. Five samples are fabricated and tested for each specimen type and loading rate, respectively, and the results are averaged. The specimens that do not contain MWCNTs are exposed to the same ultrasound sonication energy that is used to manufacture the specimens with aligned MWCNTs, to eliminate the effect of the ultrasound exposure from the comparison. The experimental results are nondimensionalized with the average ultimate tensile strength $\sigma_{\text{UTS},m}$ and the average elastic modulus E_m , respectively, of the resin material specimens without MWCNTs. Fig. 7 shows the mean $\sigma_{\text{UTS},c}/\sigma_{\text{UTS},m}$ and Fig. 8 shows the mean E_c/E_m versus the MWCNT loading rate. The error bars represent the 90% confidence interval of the respective measurements for the different specimen types. The data is tabulated in Table 2 to provide the detail that is not easily obtained from the respective figures.

Fig. 7 shows that a 6% increase of $\sigma_{\text{UTS},c}/\sigma_{\text{UTS},m}$ is obtained for an MWCNT loading rate of 0.15 wt%. However, the ultimate tensile strength decreases when increasing the MWCNT loading rate above 0.15 wt%. Specimens with aligned MWCNTs compared to randomly oriented MWCNTs do not seem to result in an increase in ultimate tensile strength of the composite material. From Fig. 8 it is observed that aligned compared to randomly oriented

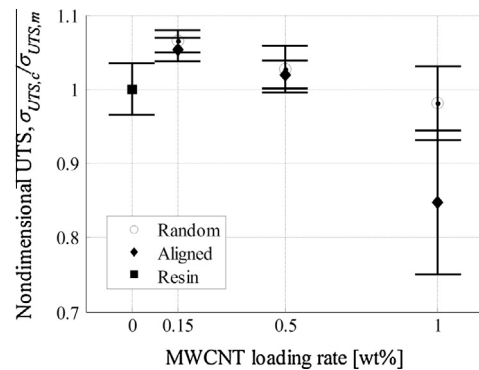


Fig. 7. Nondimensional ultimate tensile strength with 90% confidence intervals versus MWCNT loading rate (wt%), for resin specimens without MWCNTs (resin), and with randomly oriented MWCNTs (random) and aligned MWCNTs (aligned).

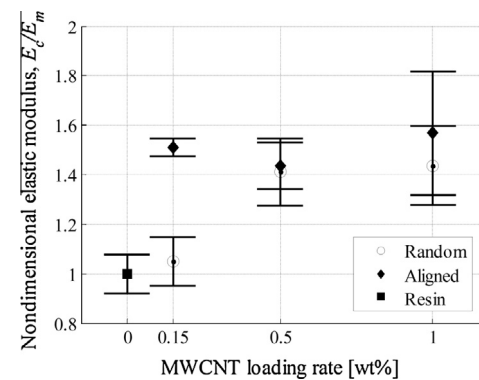


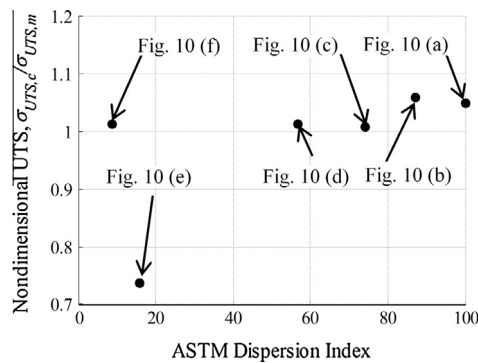
Fig. 8. Nondimensional elastic modulus with 90% confidence intervals versus MWCNT loading rate (wt%), for resin specimens without MWCNTs (resin), and with randomly oriented MWCNTs (random) and aligned MWCNTs (aligned).

MWCNTs effectively increase the elastic modulus of the composite material. Increasing the MWCNT loading rate beyond 0.15 wt% does not further increase the elastic modulus. This may indicate that dispersion of the MWCNTs in the thermoset polymer matrix is not fully achieved for loading rates in excess of 0.15 wt%. For the 0.15 wt% MWCNT loading rate, the elastic modulus of the composite material specimens with aligned MWCNTs is 44% higher than the composite material specimens with randomly oriented MWCNTs, and 51% higher than the specimens without MWCNTs. For this case, the data shows that the 90% confidence interval limits of the composite material specimens with aligned and randomly oriented MWCNTs do not overlap. The results further confirm that MWCNTs can be successfully aligned in a macroscale volume of

Table 2

Summary of static testing results shown in Figs. 7 and 8.

MWCNT loading rate (wt%)	Alignment	Average E_c/E_m Average $\sigma_{UTS,c}/\sigma_{UTS,m}$	90% Confidence interval: lower limit	90% Confidence interval: upper limit
0	–	1	0.92	1.08
0.15	Random	1	0.99	1.01
		1.05	0.95	1.15
0.15	Aligned	1.06	1.05	1.08
		1.51	1.47	1.55
0.50	Random	1.05	1.04	1.07
		1.41	1.28	1.55
0.50	Aligned	1.03	1.00	1.06
		1.44	1.34	1.53
1.00	Random	1.02	1.00	1.04
		1.44	1.28	1.60
1.00	Aligned	0.98	0.93	1.03
		1.57	1.32	1.82
		0.85	0.75	0.94

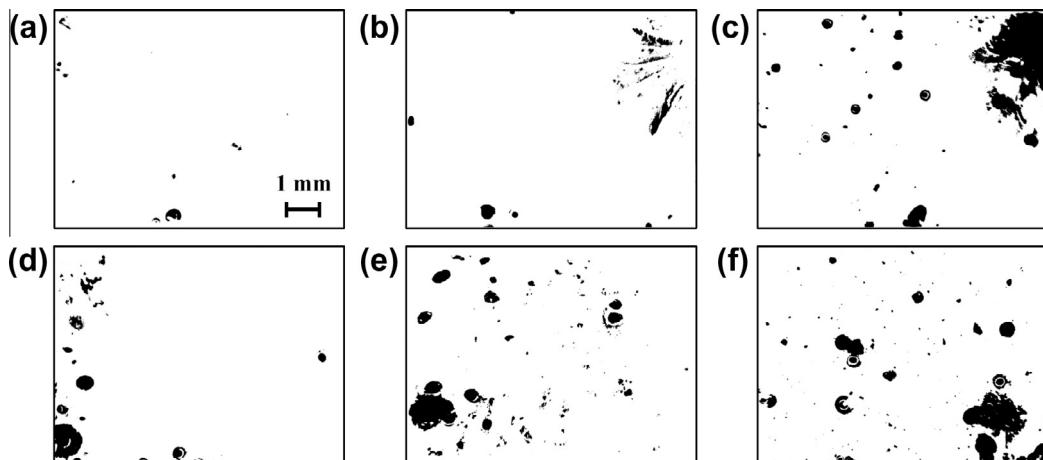
**Fig. 9.** Nondimensional ultimate tensile strength versus the ASTM dispersion index for all composite material specimens.

thermoset polymer using BAWs, thereby improving the elastic modulus of MWCNT reinforced composite materials. While the limits of the 90% confidence interval overlap for the MWCNT loading rates in excess of 0.15 wt%, an increase in elastic modulus compared to the material specimens without MWCNTs is still observed. The size of the confidence interval increases with the MWCNT loading rate, reflecting the uncertainty about the dispersion of the MWCNTs. Good dispersion is essential before the alignment is performed, such that each MWCNT can maintain intimate contact with the matrix material even after alignment

and clustering at the nodes of the standing BAW. Only then can shear stresses be effectively transferred from the polymer matrix to the MWCNT filler. Bath sonication is used for economic reasons in this work, but it is not the most efficient method to disperse MWCNTs in a polymer solution [14]. Tip sonication and/or shear mixing may yield better results.

3.3. Dispersion

We have evaluated dispersion of the MWCNTs in the hardened polymer matrix using the ASTM dispersion index (ASTM D2663-08 Method B). This index is based on the count of black pixels (carbon) in a binary image and ranges between 0 and 100, with a higher number indicating better dispersion. For the details of the ASTM dispersion index calculation, the reader is referred to the ASTM D2663-08 standard. Dispersion is quantified in the fracture surface after tensile testing of each dog-bone specimen. The fracture surface is a good location to analyze the dispersion of MWCNTs in the composite material specimen, because poor dispersion generates voids and clusters of MWCNTs that weaken the strength of the composite. Thus, a location that has the largest aggregate of MWCNTs, and therefore the poorest dispersion, will likely be the location where failure of the specimen will occur. Characterizing dispersion of MWCNTs in a polymer matrix using this ASTM index shows deficiencies [53]. More advanced methods based on dynamic light scattering and centrifugal separation analysis [54], and transmission electron microscopy [55] exist, and provide a more accurate account of the dispersion. However, to assess the dispersion of a macroscale (fracture) surface, these more advanced

**Fig. 10.** Fracture surface images that have been converted to binary with a luminance cut off of 0.20; (a) 0.15 wt% aligned, (b) 0.15 wt% random, (c) 0.5 wt% random, (d) 0.15 wt% aligned, (e) 1 wt% aligned, and (f) 0.5 wt% random.

techniques are ineffective. Nevertheless, the dispersion results obtained with the ASTM index match the visual dispersion observations well, and are useful in explaining the results of the experimental measurements of the elastic modulus and the ultimate tensile strength. Fig. 9 shows the nondimensional ultimate tensile strength of the composite material specimens, $\sigma_{UTS,c}/\sigma_{UTS,m}$, as a function of the ASTM dispersion index value obtained for selected specimens. We observe that the ultimate tensile strength increases with increasing dispersion index, providing substantiation to the speculation that insufficient dispersion hinders the increase in strength of the composite material specimens with a MWCNT loading rate larger than 0.15 wt%. The data points in Fig. 9 are labeled, and the corresponding (binary) image of the fracture surface of the dog-bone specimen is shown in Fig. 10, to visually assess the dispersion of the MWCNTs in the polymer matrix at the fracture surface. As the dispersion index decreases from Fig. 10(a–f), larger clusters of MWCNTs are observed, visually confirming the reduced dispersion. Fig. 10 shows the fracture surface of a specimen with (a) 0.15 wt% aligned MWCNTs, (b) 0.15 wt% randomly oriented MWCNTs, (c) 0.5 wt% randomly oriented MWCNTs, (d) 0.15 wt% aligned MWCNTs, (e) 1 wt% aligned MWCNTs, and (f) 0.5 wt% randomly oriented MWCNTs. Specimens with identical composition display different dispersion index results as, for instance, Fig. 10(c and f). This is expected based on the experimental measurements of the elastic modulus and ultimate tensile strength, which show that the magnitude of the error bars increased with the MWCNT loading rate (Figs. 7 and 8).

4. Conclusion

Alignment of MWCNTs in a macroscale volume of polymer material is achieved using bulk acoustic waves. The alignment method can be scaled to fabricate large composite material specimens with aligned MWCNTs, in a wide variety of shapes, and offers a possible solution to the problem of scalable manipulation and alignment of MWCNTs.

The primary limitations to this method are the viscosity and cure time of the host medium (thermoset resin), and the desired shape of the composite specimens. The types of resin that can be employed using this acoustic manipulation technique are currently limited to fast curing, ultra-low viscosity thermosets. The shape of the composite material specimens with aligned MWCNTs is limited to one with two parallel sides for the PZT transducers to establish the BAW. However, the specimen can be further machined to the desired shape following its extraction from the reservoir.

Despite the limitations of this method, the composite material specimens fabricated for this research exhibit nanoscale alignment comparable to other MWCNT alignment techniques. The alignment processing time is very fast and macroscale volumes containing dispersed MWCNTs can be aligned quasi-instantaneously. The composite material specimens fabricated using this technique with a MWCNT loading rate of 0.15 wt% demonstrate an increase of the ultimate tensile strength of 6% and an increase of the elastic modulus of 51% compared to the specimens without MWCNTs. When further increasing the MWCNT loading rate, the increase in elastic modulus remains constant while the ultimate tensile strength of the composite material decreases as a result of insufficient dispersion of the MWCNT in the resin matrix material.

References

- [1] Moniruzzaman M, Winey KI. Polymer nanocomposites containing carbon nanotubes. *Macromolecules* 2006;39:5194–205.
- [2] De Heer WA. Nanotubes and the pursuit of applications. *MRS Bull* 2004;29:281–5.
- [3] Ajayan PM, Schadler LS, Giannaris C, Rubio A. Single-walled carbon nanotube-polymer composites: strength and weakness. *Adv. Mater.* 2000;12:750–3.
- [4] Lau AKT, Hui D. The revolutionary creation of new advanced materials—carbon nanotube composites. *Composites B* 2002;33:263–77.
- [5] Gojny FH, Wichmann MHC, Köpke U, Fiedler B, Schulte K. Carbon nanotube-reinforced epoxy-composites: enhanced stiffness and fracture toughness at low nanotube content. *Compos Sci Technol* 2004;64:2363–71.
- [6] Breuer O, Sundararaj U. Big returns from small fibers: a review of polymer/carbon nanotube composites. *Polym Compos* 2004;25:630–45.
- [7] Schulte K, Gojny FH, Fiedler B, Sandler JKW, Bauhofer W. Carbon nanotube-reinforced polymers: a state of the art review. *Polym Compos* 2005;1:3–23.
- [8] Chen X, Wang J, Lin M, Zhong W, Feng T, Chen J, et al. Mechanical and thermal properties of epoxy nanocomposites reinforced with amino-functionalized multi-walled carbon nanotubes. *Mater Sci Eng A* 2008;492:236–42.
- [9] Georgakilas V, Bourlinos A, Gournis D, Tsoufis T, Trapalis C, Mateo-Alonso A, et al. Multipurpose organically modified carbon nanotubes: from functionalization to nanotube composites. *J Am Chem Soc* 2008;130:8733–40.
- [10] Suggs K, Wang XQ. Structural and electronic properties of carbon nanotube-reinforced epoxy resins. *Nanoscale* 2010;2:385–8.
- [11] Shokrieh MM, Rafiee R. Investigation of nanotube length effect on the reinforcement efficiency in carbon nanotube based composites. *Compos Struct* 2010;92:2415–20.
- [12] Chou T-W, Gao L, Thostenson ET, Zhang Z, Byun J-H. An assessment of the science and technology of carbon nanotube-based fibers and composites. *Compos Sci Technol* 2010;70:1–19.
- [13] Xie X-L, Mai Y-W, Zhou X-P. Dispersion and alignment of carbon nanotubes in polymer matrix: a review. *Mater Sci Eng R* 2005;49:89–112.
- [14] Huang YY, Terentjev EM. Dispersion of carbon nanotubes: mixing, sonication, stabilization, and composite properties. *Polymers* 2012;4:275–95.
- [15] Hwang GL, Shieh YT, Hwang KC. Efficient load transfer to polymer-grafted multiwalled carbon nanotubes in polymer composites. *Adv Funct Mater* 2004;14:487–91.
- [16] Wong M, Paramsothy M, Xu XJ, Ren Y, Li S, Liao K. Physical interactions at carbon nanotube-polymer interface. *Polymer* 2003;44(25):7757–64.
- [17] Roy D, Bhattacharyya S, Rachamim A, Plati A, Saboungi ML. Measurement of interfacial shear strength in single wall carbon nanotubes reinforced composite using Raman spectroscopy. *J Appl Phys* 2010;107:043501–0435016.
- [18] Lau K-T, Gu C, Hui D. A critical review on nanotube and nanotube/nanoclay related polymer composite materials. *Compos Part B-Eng* 2006;37(6):425–36.
- [19] Thostenson ET, Ren Z, Chou TW. Advances in the science and technology of carbon nanotubes and their composites: a review. *Compos Sci Technol* 2001;61:1899–912.
- [20] Joshi UA, Sharma SC, Harsha SP. Effect of carbon nanotube orientation on the mechanical properties of nanocomposites. *Compos Part B-Eng* 2012;43(4):2063–71.
- [21] Jin L, Bower C, Zhou O. Alignment of carbon nanotubes in a polymer matrix by mechanical stretching. *Appl Phys Lett* 1998;73(9):1197.
- [22] Fujiwara M, Oki E, Hamada M, Tanimoto Y, Mukouda I, Shimomura Y. Magnetic orientation and magnetic properties of a single carbon nanotube. *J Phys Chem A* 2001;105:4383.
- [23] Kimura T, Ago H, Tobita M, Ohshima S, Kyotani M, Yumura M. Polymer composites of carbon nanotubes aligned by a magnetic field. *Adv Mater* 2002;14:1380–3.
- [24] Shaver J, Parra-Vasquez ANG, Hansel S, Portugal O, Mielke CH, Von Ortenberg M, et al. Alignment dynamics of single-walled carbon nanotubes in pulsed ultrahigh magnetic fields. *ACS Nano* 2008;3:131–8.
- [25] Prolongo SG, Meliton BG, Del Rosario G, Ureña A. New alignment procedure of magnetite-CNT hybrid nanofillers on epoxy bulk resin with permanent magnets. *Compos Part B-Eng* 2013;46:166–72.
- [26] Fishbine BH. Carbon nanotube alignment and manipulation using electrostatic fields. *Fullerene Sci Technol* 1996;4(1):87–100.
- [27] Ajayan P, Stephan O, Colliex C, Trauth D. Aligned carbon nanotube arrays formed by cutting a polymer resin-nanotube composite. *Science* 1994;265:1212–4.
- [28] Lagerwall J, Scalia G, Haluska M, Dettlaff-Weglikowska U, Roth S, Giesselmann F. Nanotube alignment using lyotropic liquid crystals. *Adv Mater* 2007;19:359–64.
- [29] Fan Z, Advani SG. Characterization of orientation state of carbon nanotubes in shear flow. *Polymer* 2005;46:5232–40.
- [30] Strobl CJ, Schaflein C, Beierlein U, Ebbecke J, Wixforth A. Carbon nanotube alignment by surface acoustic waves. *Appl Phys Lett* 2004;85:1427.
- [31] Zhang S, Koziol KK, Kinloch IA, Windle AH. Macroscopic fibers of well-aligned carbon nanotubes by wet spinning. *Small* 2008;4:1217–22.
- [32] Haggenueller R, Gommans H, Rinzler A, Fischer JE, Winey K. Aligned single-wall carbon nanotubes in composites by melt processing methods. *Chem Phys Lett* 2000;330:219–25.
- [33] Pötschke P, Brüning H, Janke A, Fischer D, Jehnichen D. Orientation of multiwalled carbon nanotubes in composites with polycarbonate by melt spinning. *Polymer* 2005;46:10355–63.
- [34] Gao J, Itkis ME, Yu A, Bekyarova E, Zhao B, Haddon RC. Continuous spinning of a single-walled carbon nanotube-nylon composite fiber. *J Am Chem Soc* 2005;127:3847–54.
- [35] Li YL, Kinloch IA, Windle AH. Direct spinning of carbon nanotube fibers from chemical vapor deposition synthesis. *Science* 2004;304:276.
- [36] Coakley W, Hawkes J, Sobanski M, Cousins C, Spengler J. Analytical scale ultrasonic standing wave manipulation of cells and microparticles. *Ultrasonics* 2000;38:638–41.

- [37] Haake A, Dual J. Micro-manipulation of small particles by node position control of an ultrasonic standing wave. *Ultrasonics* 2002;40:317–22.
- [38] Oberti S, Neild A, Möller D, Dual J. Towards the automation of micron-sized particle handling by use of acoustic manipulation assisted by microfluidics. *Ultrasonics* 2008;48:529–36.
- [39] Greenhall JJ, Guevara Vasquez F, Raeymaekers B. Continuous and unconstrained manipulation of micro-particles using phase-control of bulk acoustic waves. *Appl Phys Lett* 2013;103:074103.
- [40] Haake A, Neild A, Kim DH, Ihm JE, Sun Y, Dual J, et al. Manipulation of cells using an ultrasonic pressure field. *Ultrasound Med Biol* 2005;31:857–64.
- [41] Coakley W, Whitworth G, Grundy M, Gould R, Allman R. Ultrasonic manipulation of particles and cells, ultrasonic separation of cells. *Bioseparation* 1994;4:73.
- [42] Raeymaekers B, Pantea C, Sinha DN. Manipulation of diamond nanoparticles using bulk acoustic waves. *J Appl Phys* 2011;109:014317.
- [43] Du Toit F, Sanderson R, Engelbrecht W, Wagener J. The effect of surface fluorination on the wettability of high density polyethylene. *J Fluorine Chem* 1995;74:43–8.
- [44] Mitri FG. Theoretical calculation of the acoustic radiation force acting on elastic and viscoelastic cylinders placed in a plane standing or quasistanding wave field. *Eur Phys J B* 2005;44:71–8.
- [45] Wu J, Du G, Work SS, Warsaw DM. Acoustic radiation pressure on a rigid cylinder: an analytical theory and experiments. *J Acoust Soc Am* 1990;87:581–6.
- [46] Wei W, Thiessen DB, Marston PL. Acoustic radiation force on a compressible cylinder in a standing wave. *J Acoust Soc Am* 2004;116:201.
- [47] Haydock D. Calculation of the radiation force on a cylinder in a standing wave acoustic field. *J Phys A* 2005;38:3279–85.
- [48] Kinsler LE, Frey AR. *Fundamentals of acoustics*. New York: J. Wiley & Sons; 1962.
- [49] Hermans J, Hermans P, Vermaas D, Weidinger A. Quantitative evaluation of orientation in cellulose fibres from the X-ray fibre diagram. *Recl Trav Chim Pay-B* 1946;65:427–47.
- [50] Bhattacharyya AR, Sreekumar T, Liu T, Kumar S, Ericson LM, Hauge RH, et al. Crystallization and orientation studies in polypropylene/single wall carbon nanotube composite. *Polymer* 2003;2003(44):2373–7.
- [51] Zhang S, Koziol KK, Kinloch IA, Windle AH. Macroscopic fibers of well-aligned carbon nanotubes by wet spinning. *Small* 2008;4:1217–22.
- [52] Koerner H, Price G, Pearce NA, Alexander M, Vaia RA. Remotely actuated polymer nanocomposites—stress-recovery of carbon-nanotube-filled thermoplastic elastomers. *Nat Mater* 2004;3:115–20.
- [53] Haslam MD, Raeymaekers B. A composite index to quantify dispersion of carbon nanotubes in polymer-based composite materials. *Compos Part B-Eng* 2013;55:16–21.
- [54] Krause B, Mende M, Pötschke P, Petzold G. Dispersability and particle size distribution of CNTs in an aqueous surfactant dispersion as a function of ultrasonic treatment time. *Carbon* 2010;48:2746–54.
- [55] Mueller MT, Krause B, Poetschke P. A successful approach to disperse MWCNTs in polyethylene by melt mixing using polyethylene glycol as additive. *Polymer* 2012;53(15):3079–83.